© 2022. Published by The Company of Biologists Ltd | Development (2022) 149, dev200016. doi:10.1242/dev.200016

HUMAN DEVELOPMENT

TECHNIQUES AND RESOURCES ARTICLE

Derivation of extra-embryonic and intra-embryonic macrophage lineages from human pluripotent stem cells

Andrea L. Bredemeyer[1], Junedh M. Amrute[1], Andrew L. Koenig[1], Rachel A. Idol[2], Li He[1], Stephanie A. Luff[3,4], Carissa Dege[5], Jamison M. Leid[1], Joel D. Schilling[1], J. Travis Hinson[6,7], Mary C. Dinauer[2], Christopher M. Sturgeon[3,4,5,*] and Kory J. Lavine[1,8,9,*]

ABSTRACT

Tissue-resident macrophages are increasingly recognized as important determinants of organ homeostasis, tissue repair, remodeling and regeneration. Although the ontogeny and function of tissue-resident macrophages has been identified as distinct from postnatal hematopoiesis, the inability to specify, *in vitro*, similar populations that recapitulate these developmental waves has limited our ability to study their function and potential for regenerative applications. We took advantage of the concept that tissue-resident macrophages and monocyte-derived macrophages originate from distinct extra-embryonic and definitive hematopoietic lineages to devise a system to generate pure cultures of macrophages that resemble tissue-resident or monocyte-derived subsets. We demonstrate that human pluripotent stem cell-derived extra-embryonic-like and intra-embryonic-like hematopoietic progenitors differentiate into morphologically, transcriptionally and functionally distinct macrophage populations. Single-cell RNA sequencing of developing and mature cultures uncovered distinct developmental trajectories and gene expression programs of macrophages derived from extra-embryonic-like and intra-embryonic-like hematopoietic progenitors. These findings establish a resource for the generation of human tissue resident-like macrophages to study their specification and function under defined conditions and to explore their potential use in tissue engineering and regenerative medicine applications.

KEY WORDS: Macrophages, Hematopoiesis, Tissue-resident macrophages, Human pluripotent stem cells

[1]Center for Cardiovascular Research, Departmental of Medicine, Cardiovascular Division, Washington University School of Medicine, St Louis, MO 63110, USA. [2]Department of Pediatrics, Washington University School of Medicine, St Louis, MO 63110, USA. [3]Department of Cell, Developmental and Regenerative Biology, Icahn School of Medicine at Mount Sinai, New York, NY 10029, USA. [4]Black Family Stem Cell Institute, Icahn School of Medicine at Mount Sinai School of Medicine, New York, NY 10029, USA. [5]Department of Medicine, Division of Hematology, Washington University School of Medicine, St Louis, MO 63110, USA. [6]Departments of Cardiology, Genetics and Genome Sciences, UConn Health, Farmington, CT 06030, USA. [7]The Jackson Laboratory for Genomic Medicine, Farmington, CT 06032, USA. [8]Department of Pathology and Immunology, Washington University School of Medicine, St Louis, MO 63110, USA. [9]Department of Developmental Biology, Washington University School of Medicine, St Louis, MO 63110, USA.

*Authors for correspondence (christopher.sturgeon@mssm.edu; klavine@wustl.edu)

A.L.B., 0000-0003-2970-5998; A.L.K., 0000-0003-4384-1267; R.A.I., 0000-0002-7043-6630; J.M.L., 0000-0002-3137-6583; J.D.S., 0000-0002-3884-1994; J.T.H., 0000-0003-1455-113X; M.C.D., 0000-0002-7796-2908; C.M.S., 0000-0003-1508-4414; K.J.L., 0000-0003-1948-9945

Handling Editor: Hanna Mikkola
Received 15 July 2021; Accepted 31 January 2022

INTRODUCTION

Macrophages are well appreciated for their roles in pathogen responses, including phagocytosis of pathogens and removal of cellular debris, release of inflammatory cytokines, and presentation of antigen to cells of the adaptive immune system (Murray and Wynn, 2011). Over the last ten years, however, the impact of macrophages residing within tissues on organ homeostasis and repair has become increasingly understood. Studies of resident macrophages across various tissues have revealed common functions, such as promotion of angiogenesis and proper tissue patterning during development (Wynn et al., 2013). Each tissue environment also instructs macrophages to take on specific functional properties, leading to specialization of microglia in the brain, Kupffer cells in the liver, Langerhans cells in the skin and osteoclasts in the bone (Epelman et al., 2014b; Davies et al., 2013; Lavin et al., 2014).

Tissue-resident macrophages are initially derived from the hematopoietic progenitors arising in the extra-embryonic yolk sac (Hoeffel and Ginhoux, 2015; Hoeffel et al., 2015; Ginhoux et al., 2010; Yona et al., 2013). During early embryogenesis, these extra-embryonic cells migrate to developing tissues where they establish their tissue-specific identity. Over the course of fetal development and postnatal life, these tissue-resident macrophages have the capacity to self-renew and are maintained in the absence of replenishment from monocytes in many tissues, including liver, lung, brain and heart (Hashimoto et al., 2013; Epelman et al., 2014a; Ajami et al., 2007). Similarly, upon physiological stressors, such as injury or aging, monocyte-derived macrophages can migrate to these tissues and function as tissue-resident macrophages (Epelman et al., 2014a; Daemen et al., 2021). However, these ontogenically distinct macrophages generally lack the reparative functions of their extra-embryonic-derived counterparts, instead causing inflammation that can contribute to disease phenotypes (Honold and Nahrendorf, 2018; Puranik et al., 2018).

Extra-embryonic hematopoiesis in the yolk sac occurs in at least two waves, the first consisting of primitive, MYB-independent progenitors that give rise to a very limited set of hematopoietic cells (primitive erythroblasts, megakaryocytes and macrophages) and the second consisting of MYB-dependent erythromyeloid progenitors (EMPs) that give rise to erythroid, myeloid and natural killer cell lineages (Dege et al., 2020; Frame et al., 2013; Kasaai et al., 2017; McGrath et al., 2015; Palis et al., 1995; Palis et al., 1999; Palis and Yoder, 2001; Lux et al., 2008). EMPs provide the first progenitors that colonize the fetal liver, giving rise to diverse myeloid cells. In contrast, the intra-embryonic hemogenic endothelium within the aorta-gonad-mesonephros (AGM) region gives rise to definitive multipotent progenitors (MPPs) and hematopoietic stem cells (HSCs). These long-lived HSCs migrate to the fetal liver, and finally the bone marrow, to produce a full assortment of myeloid and lymphoid cells.

Development (2022) 149, dev200016. doi:10.1242/dev.200016

In order to assess the intrinsic differences between hematopoietic lineages arising from extra- and intra-embryonic hematopoiesis, we developed an *in vitro* human pluripotent stem cell (hPSC) differentiation model of hematopoiesis that recapitulates these anatomically distinct hematopoietic programs. By manipulating WNT signaling at an early stage of differentiation, we can generate either exclusively extra-embryonic-like (WNT-independent, WNTi) $CD34^+$ hematopoietic progenitors, or exclusively intra-embryonic-like (WNT-dependent, WNTd) $CD34^+$ hematopoietic progenitors (Sturgeon et al., 2014). WNTi progenitors lack the expression of *HOXA* genes and have restricted erythro-myeloid potential, mirroring extra-embryonic hematopoiesis, whereas WNTd progenitors express *HOXA*, and display multi-lineage erythro-myelo-lymphoid potential, recapitulating intra-embryonic-like MPP development (Ng et al., 2016).

Here, we present a platform to generate two ontogenically distinct myeloid populations from hPSCs. Through our ability to directly compare each population from a single isogenic source, we demonstrate that macrophages differentiated from extra-embryonic-like (WNTi) and intra-embryonic-like (WNTd) hematopoietic progenitors harbor distinct transcriptional signatures, morphologies, developmental pathways, and functions, which recapitulate the general properties observed in yolk sac-derived and intra-embryonic macrophages, respectively. These findings establish a robust *in vitro* system for generating functionally distinct myeloid populations for investigation of human macrophage specification, differentiation, function and regenerative potential.

RESULTS

Generation of macrophages derived from extra-embryonic- and intraembryonic-like hematopoietic progenitors

Using previously described conditions to exclusively specify extra-embryonic-like and intra-embryonic-like hematopoietic progenitors from hPSCs, we sought to determine whether we could generate functional macrophages in these lineages (Fig. 1A). Consistent with previous findings, differentiation under WNTi conditions (IWP2 treatment) gave rise to $CD34^+$ progenitors that rapidly transitioned to CD43 (SPN)$^+$ hematopoietic progenitors by day 8 of differentiation. Within these cultures, $CD34^-CD43^+$ cells displayed predominantly erythroid potential, whereas $CD34^+CD43^+$ cells instead harbored robust myeloid potential, identifying them as a candidate population of extra-embryonic-like macrophage progenitors (Fig. S1A,B). In contrast, treatment with the GSK3 inhibitor CHIR99021, which activates WNT (and consequently Notch) signaling, and the TGFβ inhibitor SB-431542 (called WNTd conditions here for simplicity), yields $CD34^+CD43^-CD73$ (NT5E)$^-$CD184 (CXCR4)$^-$ hemogenic endothelial cells on day 8 of differentiation, which possess intra-embryonic-like erythroid, myeloid and lymphoid multipotent potential (Ditadi et al., 2015; Ng et al., 2016).

WNTi $CD34^+CD43^+$, WNTd $CD34^+CD43^-CD73^-CD184^-$ and human cord blood (CB) $CD34^+$ populations were isolated by fluorescence-activated cell sorting (FACS), then cultured under serum-free conditions supplemented with M-CSF (CSF1) and additional cytokines to drive macrophage differentiation (Fig. S1A). CB $CD34^+$ hematopoietic progenitors were used as a control for definitive hematopoiesis. After 14 days, the cultures were analyzed by flow cytometry for expression of the leukocyte marker CD45 (PTPRC) and common macrophage markers. Differentiation in all cultures was highly efficient, as over 90% of the cells expressed CD45 and the macrophage markers CD14 and MERTK (Fig. 1B). The WNTd culture yielded an average of 2×10^6 macrophages per 1×10^5 purified progenitors, whereas the WNTi culture averaged 1×10^6 macrophages per 1×10^5 sorted progenitors. WNTi and WNTd cultures were each generated from 5×10^6 hPSCs. Whereas the cells within the WNTd- and CB-derived cultures had similar scatter properties, WNTi-derived cells displayed higher median forward scatter (FSC) and side scatter (SSC) (Fig. 1C, Fig. S1C). We also examined CCR2 expression in each population, as its expression on tissue-resident macrophages correlates with an intra-embryonic, but not extra-embryonic, origin (Bajpai et al., 2018; Epelman et al., 2014a). Consistent with an extra-embryonic-like origin, WNTi $CD45^+CD14^+$ cells were completely devoid of CCR2 expression, whereas the WNTd- and CB-derived cells both exhibited $CCR2^+$ and $CCR2^-$ subsets (Fig. 1D). Electron microscopy revealed that the cells from each culture contained morphological elements typical of macrophages, including phagosomes, lysosomes and pseudopodia (Fig. 1E). Finally, we assessed the phagocytosis efficiency of each population by culturing the cells with pHrodo Red *Escherichia coli* BioParticles, which will only fluoresce in low pH phagosomes. Both the WNTi and WNTd macrophages had similar percentages (comparable to CB-derived macrophages) and levels of pHrodo Red positivity, demonstrating comparable phagocytic capacity for *E. coli* particles (Fig. 1F, Fig. S1D). Collectively, these phenotypic analyses indicate that each $CD45^+$ population comprises macrophages, with hPSC-derived WNTd macrophages displaying strong similarity to those derived from CB HSPCs, whereas WNTi macrophages are phenotypically unique.

Distinct transcriptomic signatures in WNTi and WNTd macrophages

Monocyte-derived macrophages and yolk-sac-derived tissue-resident macrophages have distinct gene expression profiles. However, the extent to which these gene expression differences are cell intrinsic or driven by their environment remains incompletely understood. As our *in vitro* platform yields macrophages from extra- and intra-embryonic-like progenitors, we investigated whether each population harbors gene expression differences, at single-cell resolution. From macrophage day 14 cultures, 11,113 cells were captured for single-cell RNA sequencing (scRNAseq). Both WNTd and WNTi samples had comparable numbers of genes and unique molecular identifiers (UMIs) per cell (Fig. S2A). Unsupervised clustering of the WNTi and WNTd macrophages together by uniform manifold approximation and projection (UMAP) identified 12 cell clusters, with the WNTd and WNTi cells predominantly segregating into distinct groups of clusters (Fig. 2A,B, Fig. S2B). Differentially expressed genes (DEGs) within each cluster allowed for the identification of cell fate (Fig. 2C, Table S1). Although most cells were in G0/G1 across both datasets, we also identified a separate cluster with enriched expression of S/G2/M-associated genes [*TOP2A*, *KIAA0101* (*PCLAF*), *MKI67*, *CDK1*; Fig. 2B,C, Fig. S2B,C].

Macrophages were identified based on expression of *SPP1*, *C1QA*, *C1QB* and *C1QC* and made up most clusters in both the WNTi and WNTd populations (Fig. 2C). The WNTd and WNTi macrophages also expressed comparable levels of *MAF*, *MAFB*, *CD68*, *CD163* and *MRC1* (Fig. S2D,E). In contrast, a cluster of cells expressing characteristic monocyte genes (*FCN1*, *CD52*, *LYZ* and *PLAC8*), as well as CCR2, was found exclusively in the WNTd culture (Fig. 2C, Fig. S2F). We also identified a small cluster expressing mast cell genes (*KIT*, *TPSB2*, *CPA3*, *HPGD*) in the WNTi culture. At a broad level, the WNTd and WNTi macrophages each expressed a distinct gene signature that spanned all their respective clusters (Fig. 2D,E, Fig. S3). Interestingly, the WNTi

Development (2022) 149, dev200016. doi:10.1242/dev.200016

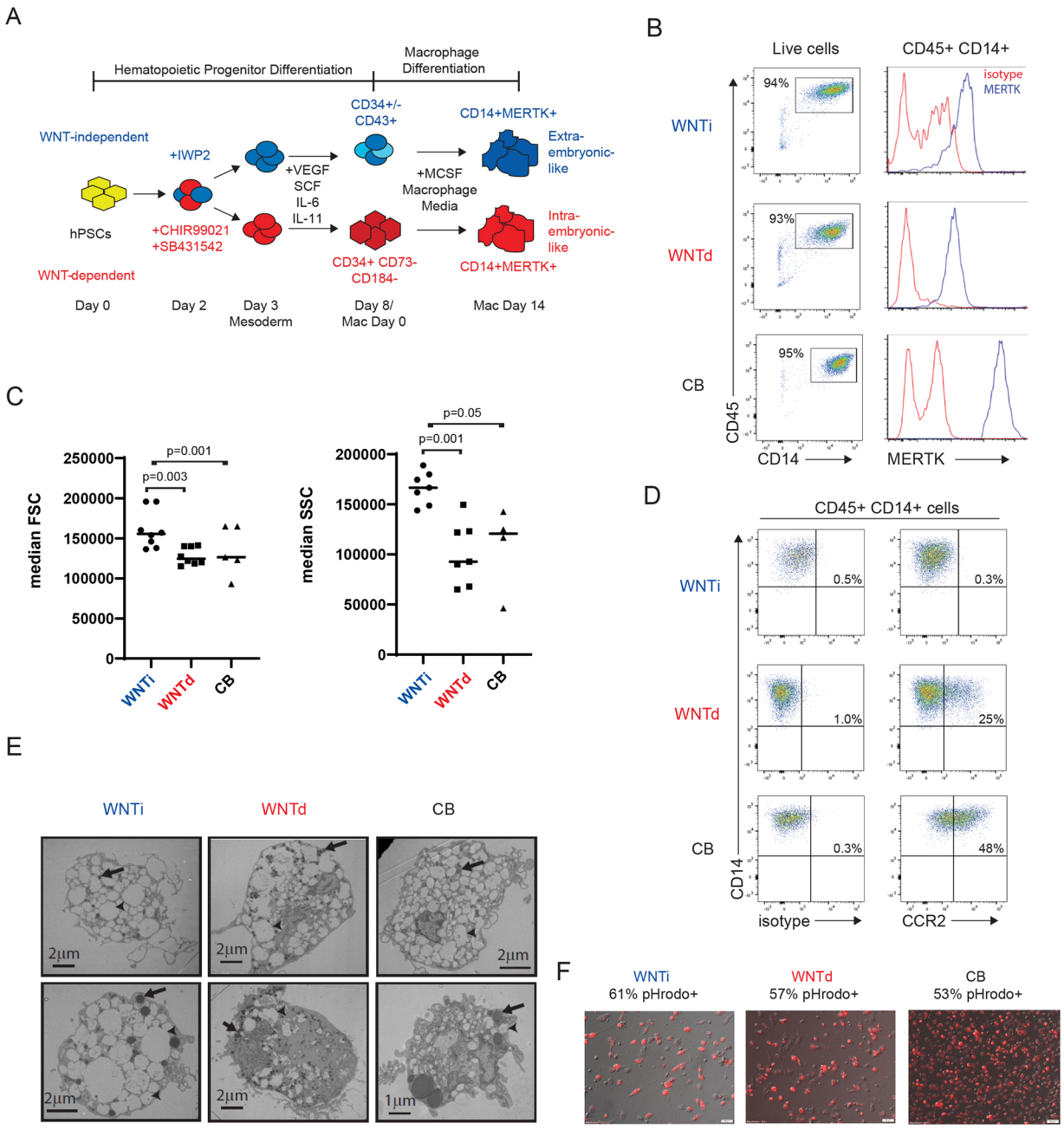

Fig. 1. Generation and characterization of WNTi and WNTd hPSC-derived macrophages. (A) Schematic of the macrophage differentiation protocol. (B) Representative flow cytometric analysis of the leukocyte marker CD45 and the macrophage markers CD14 and MERTK on WNTi, WNTd and CB cells after 14 days in macrophage media. (C) Quantification of median FSC and SSC of CD14$^+$ cells from four to seven independent differentiations. Two-tailed Student's *t*-test. (D) Flow cytometric analysis of CCR2 expression on WNTi, WNTd and CB macrophages. Plots are representative of three independent experiments. (E) Electron microscopy of WNTi, WNTd and CB macrophages. Arrowheads indicate examples of endosomes, arrows indicate examples of lysosomes. (F) Phagocytosis of pHrodo Red *E. coli* particles by WNTi, WNTd and CB macrophages after 1 h of co-culture, as indicated by red fluorescence. Images shown are merged brightfield and fluorescence. At least 100 cells were analyzed per experiment. Images shown are representative of three independent experiments.

macrophage signature includes *LYVE1*, *F13A1*, *GAS6*, *FOLR2*, *IGFBP4* and *CD36*, genes that are enriched in a variety of tissue-resident macrophages (Summers et al., 2020). The WNTd macrophages, in contrast, expressed a broader repertoire of macrophage-associated genes that regulate function in disease states, such as *TREM2*, *BTG1*, *ALDH2*, *ALOX5AP* and *BNIP3* (Fig. 2D,E, Fig. S3) (Corjay et al., 1998; Zhong et al., 2019; Ee et al., 2016; Bäck et al., 2007; Byrum et al., 1997; Frank et al., 2015; Zhang and Ney, 2009). In particular, TREM2 is expressed on macrophages in a variety of disease contexts, including cancer and atherosclerosis, so it is intriguing to find it present across the WNTd macrophage population (Cochain et al., 2018; Deczkowska et al., 2020; Katzenelenbogen et al., 2020). Differences in protein expression of LYVE1 and TREM2 were confirmed by immunofluorescence (Fig. S4A,B). KEGG pathway analysis revealed differences in lysosomal, inflammatory, metabolic, and protein synthetic processes between WNTi and WNTd macrophage populations (Fig. 2F).

We identified each macrophage cluster by the top DEG (Fig. 2B, G, Table S1). The WNTd culture contained five clusters of cells

Development (2022) 149, dev200016. doi:10.1242/dev.200016

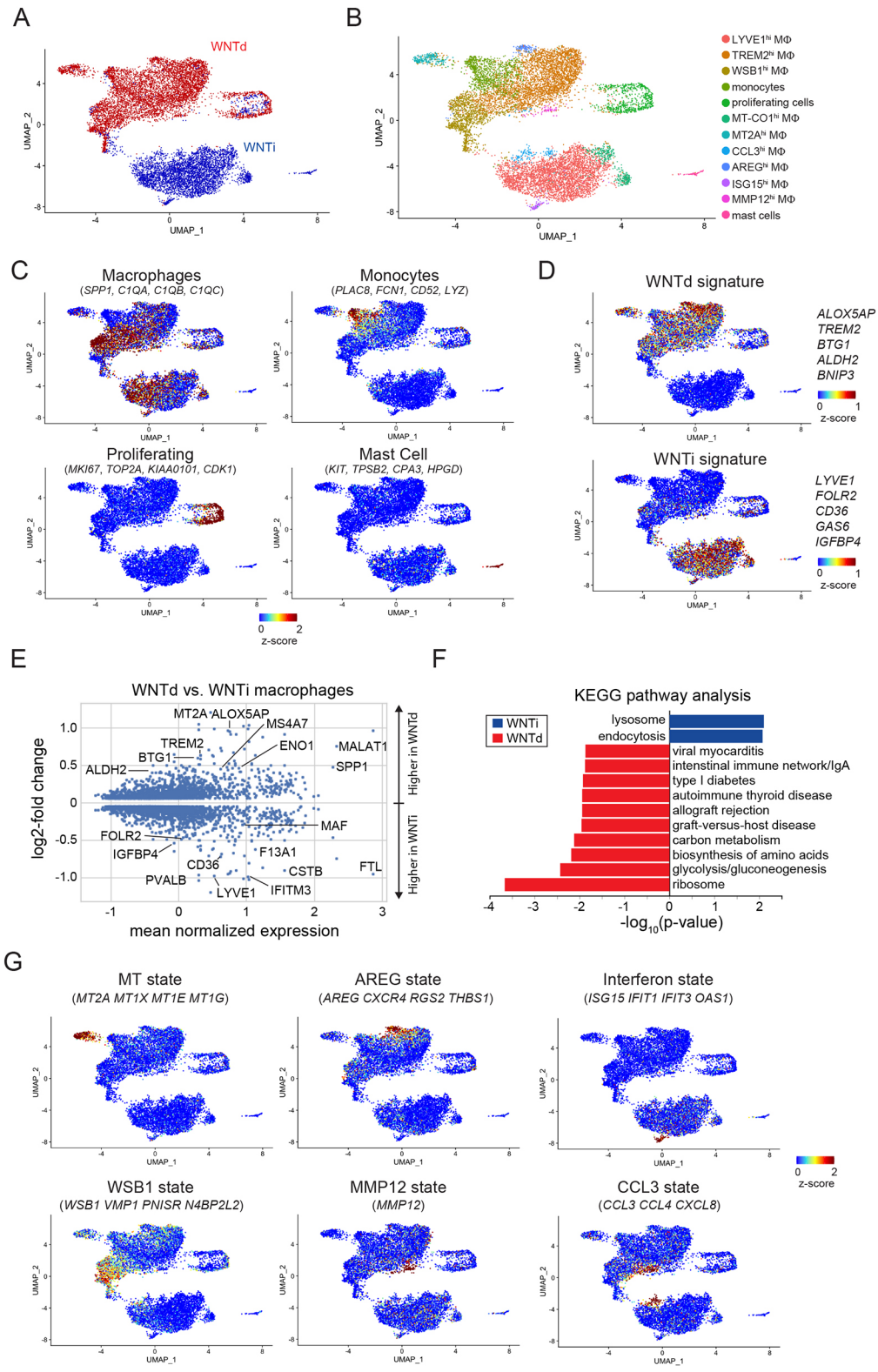

Fig. 2. scRNAseq of WNTi and WNTd macrophages. (A,B) UMAP plots of WNTd and WNTi macrophage scRNAseq. In A, WNTi cells are blue and WNTd cells are red. B shows the identity of the clusters. Each macrophage cluster is labeled with the top DEG unique to that cluster. (C) *z*-score feature plots for each distinct cell type (and proliferating cells). Genes used to calculate the *z*-score are indicated above each plot. (D) *z*-score feature plots of the WNTd and WNTi macrophage gene signatures. Genes used to calculate the *z*-score are indicated to the right of the plots. See Fig. S3 for violin plots of the individual genes. (E) MA plot of log2 fold-change versus mean normalized gene expression between WNTd and WNTi macrophages. (F) Gene set enrichment analysis for KEGG pathway database showing pathways overrepresented in WNTd and WNTi macrophages. (G) *z*-score feature plots for each macrophage state. The top DEGs, which were used to generate the *z*-scores, are indicated above the plots.

with distinct gene expression signatures, revealing the variety of fates these cells can take on. The *TREM2*^{hi} macrophage cluster expresses the WNTd signature described above, without an additional unique set of genes, suggesting that this may be the initial state of the WNTd macrophages. The cells in the metallothionein (MT) state express high levels of metallothionein 1 and 2 (MT1 and MT2) genes, which can promote inflammatory responses to pathogens (Subramanian Vignesh and Deepe, 2017). The amphiregulin (*AREG*) cluster expresses a set of genes (*AREG*, *THBS1*, *RGS2*, *ABHD2*) that have been shown to promote wound healing and angiogenesis in different tissue injury contexts (Hamidzadeh et al., 2020; Minutti et al., 2019; Zaiss et al., 2015; Kyriakides and Maclauchlan, 2009; Boelte et al., 2011; Jin et al., 2009). The *WSB1* (WD repeat and SOCS box containing 1) cluster

Development (2022) 149, dev200016. doi:10.1242/dev.200016

is also characterized by the expression of genes (*WSB1*, *PNISR*, *VMP1*, *N4BP2L2*) that can modulate immune responses and cellular function, including response to hypoxia and autophagy (Grasso et al., 2011; Haque et al., 2016). The MMP12 cluster is characterized almost entirely by expression of *MMP12*, a protease involved in macrophage migration, which is not expressed in the other clusters (Collison, 2018).

WNTi macrophages were predominantly contained in a single major cluster (*LYVE1*^{hi}) expressing the WNTi signature discussed above, with minor clusters (<5% of cells) also expressing higher levels of type 1 interferon stimulated genes (interferon state) or chemokines CCL3, CCL4 and CXCL8 (CCL3 state) (Fig. 2B,G). The WNTi macrophages also had a small cluster expressing increased levels of a subset of mitochondrially encoded genes (Fig. S4C). Analysis of variation in gene expression within the WNTd and WNTi macrophages revealed greater heterogeneity in gene expression in the WNTd macrophages, suggesting that WNTd macrophages can take on a larger number of gene expression states than the WNTi macrophages, reminiscent of the wide variety of fates recruited macrophages take on in response to tissue injury and disease (Fig. S4D) (Bajpai and Lavine, 2019; Bajpai et al., 2018). Taken together, these observations demonstrate that the WNTi and WNTd macrophages we obtain exhibit different intrinsic gene expression programs, and that these differences parallel those observed between macrophages derived from extra-embryonic and intra-embryonic hematopoietic programs *in vivo*.

Differing developmental pathways underlie the specification of WNTi and WNTd myeloid progenitors

In vivo, extra- and intra-embryonic macrophages follow distinct developmental trajectories, with only intra-embryonic myelopoiesis developing through a monocyte stage. As our scRNAseq analyses showed that WNTd, but not WNTi, macrophage cultures contained a monocytic-like precursor, we next investigated whether the hPSC myeloid populations we obtain exhibit a similar developmental progression. First, we analyzed the expression of the common monocyte and macrophage markers CD64 (FCGR1A) and CD14 on the developing macrophage cultures, from days 5 to 7, as these time points captured developmental intermediates not present in our terminally differentiated cultures. Both cultures exhibited an asynchronous maturational profile, consisting of CD64^{-}CD14^{-}, CD64^{+}CD14^{-} and CD64^{+}CD14^{+} populations (Fig. 3A). WNTd progenitors exhibited a progressive development through successive stages, first acquiring CD64 expression and then CD14, as suggested by their relative distribution over time. The distribution of these populations remained relatively static in the WNTi cultures at these time points, with a slight increase in CD64^{-}CD14^{-} cells and a decrease in CD64^{+}CD14^{-} cells, making it difficult to assess the relationships between these populations using these markers.

To characterize their development further, we assessed each population for the expression of IL3Rα (CD123), which is expressed on common myeloid progenitors (CMPs), and for CD45RA, which is expressed together with IL3Rα on downstream granulocyte/macrophage progenitors (GMPs; Manz et al., 2002). Consistent with our assessment of WNTd culture maturation, the CD64^{-}CD14^{-} cells predominantly expressed only IL3Rα, as observed in CMPs, whereas the majority of the CD64^{+}CD14^{-} cells expressed both IL3Rα and CD45RA, similar to GMPs. The fully committed CD64^{+}CD14^{+} cells all expressed both IL3Rα and CD45RA (Fig. 3B). The pattern of IL3Rα and CD45RA expression differed, however, in the WNTi culture. The CD64^{-}CD14^{-} population was predominantly negative for IL3Rα and CD45RA, whereas approximately half of the CD64^{+}CD14^{-} cells expressed IL3Rα. Intriguingly, CD45RA was not detected in either CD14^{-} population, although the CD64^{+}CD14^{+} macrophages expressed high levels of both IL3Rα and CD45RA (Fig. 3B). Exclusion of erythroid [CD235A (GYPA)$^{+}$] and megakaryocyte (CLEC1B^{+}) lineage cells increased the percentage of IL3Rα^{+} cells, but failed to increase the percentage of CD45RA^{+} progenitors (Fig. S5A). As this expression pattern suggested an absence of a canonical GMP-like stage, we also assessed an earlier time point of myeloid development. At day 3, fewer than 5% of the cells were CD64^{+}CD14^{+} macrophages, indicating that the macrophage progenitors were still present in the culture. Analysis of the CD14^{-} cells showed that about 40% expressed IL3Rα and all were negative for CD45RA (Fig. S5B). These results suggest that the WNTi macrophage progenitors either do not pass through a canonical GMP progenitor state, or that they pass through this state too rapidly to be detected by flow cytometry.

To assess the differences between WNTd and WNTi progenitors further, we performed scRNAseq on each culture after 6 days in macrophage-inducing media. Based on our flow cytometry, we predicted that both cultures would contain a mixture of cells at different stages of differentiation at this time point. We obtained data on 4217 and 6994 cells for these WNTi and WNTd progenitor cultures, respectively. Both samples had comparable numbers of genes and UMIs identified per cell (Fig. S6A). Using unsupervised clustering of the WNTi and WNTd samples together, we identified 12 distinct clusters (Fig. 3C,D). We assigned cluster identities using markers characteristic of hematopoietic cell types and verified them by reference mapping our datasets to integrated human yolk sac and fetal liver scRNAseq data (Fig. 3E, Fig. S6B-D, Fig. S7A) (Bagger et al., 2019; Popescu et al., 2019). We also examined gene expression of *IL3RA*, *FCGR1A* and *CD14* to correlate the scRNAseq data with our flow cytometry populations, and the proliferation markers *MKI67* and *TOP2A* to ensure cell cycle regression was successful (Fig. S7B,C). At this early stage of differentiation, multiple cell types were present in both cultures, giving insight into the overall potential of the WNTd and WNTi progenitors. Both cultures contained clusters expressing canonical monocyte (*PLAC8*, *LSP1*, *ASGR2*, *CORO1A*) and macrophage (*SPP1*, *VSIG4*, *C1QA*, *C1QB*, *C1QC*) genes; the majority of the WNTd culture and a smaller fraction of the WNTi culture comprised these clusters (Fig. 3C-F, Fig. S6B,C, Table S2). None of these clusters expressed high levels of *FUT4*, the gene encoding the neutrophil marker CD15 (Fig. S7B). The macrophages present in the WNTi culture predominantly clustered into the Mac-1 cluster. These express higher levels of several genes (including *LYVE1*, *SIGLEC1*, *LILRB5*, *F13A1*, *CD163* and *DAB2*) than the predominantly WNTd Mac-2 cluster, demonstrating that their gene expression signatures diverge early in macrophage maturation (Fig. 3C-F, Fig. S6C). Both cultures also had cells expressing characteristic eosinophil genes (*CLC*, *IL5RA*, *EPX*, *PRG2*, *PRG3*). Megakaryocyte (*GP9*, *ITGA2B*, *PDLIM1* and *PF4*) and mast cell (*KIT*, *TPSB2* and *GATA2*) clusters were present primarily in the WNTi culture (Fig. 3C-F, Fig. S6B,D). Similarly, the WNTi culture contained a large number of red blood cell (RBC) progenitors, expressing glycophorin A (*GYPA*), *GATA1* and *KLF*, which were largely absent from the WNTd culture, consistent with an EPO-independent development of the primitive erythroid lineage (Malik et al., 2013). Only the WNTd culture contained a cluster expressing canonical dendritic cell genes (*CD1C*, *FGL2*, *ITGB7*, *CLEC4A* and *HLA-DRA*), as well as a CD34^{+} progenitor cluster that

Development (2022) 149, dev200016. doi:10.1242/dev.200016

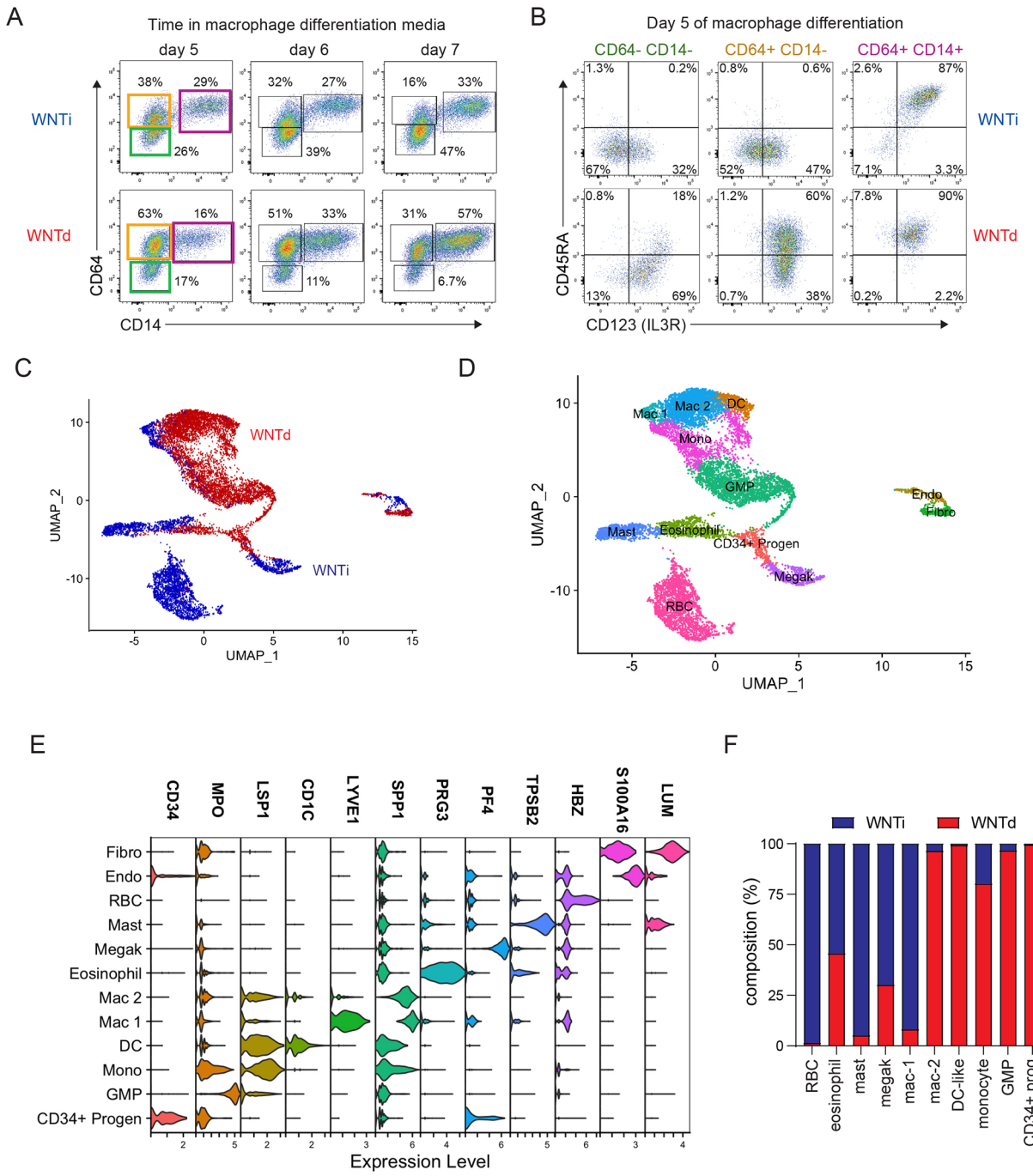

Fig. 3. WNTi and WNTd progenitors differ in cell-surface markers and downstream cell-type potential. (A) Representative flow cytometric time course of CD14 and CD64 on WNTi and WNTd progenitors. (B) IL3Rα and CD45RA expression on the indicated populations from the day 5 plots in A. (C,D) UMAP plots of WNTi and WNTd progenitor scRNAseq. In C, WNTi cells and WNTd cells are blue and red, respectively. In D, clusters are labeled based on expression of cell-type characteristic genes. (E) Violin plots of a characteristic gene for each indicated cell type. Additional expression data are shown in Fig. S6 and Table S2. (F) The percentage of WNTi and WNTd cells making up each cluster in D. DC, dendritic cells; Endo, endothelial cells; Fibro, fibroblasts; Mac, macrophages; Megak, megakaryocytes; Mono, monocytes; Progen, progenitors.

expresses characteristic intra-embryonic MPP genes (*MECOM*, *SPINK2*, *MLLT3*, *HLF*) (Figs S6D and S7D) (Kataoka et al., 2011; Zeng et al., 2019; Pina et al., 2008; Yokomizo et al., 2019). To verify that the WNTd culture represents intra-embryonic-like hematopoiesis, we reference mapped human fetal liver HSC/MPPs and yolk sac MPPs onto our WNTd progenitor dataset (Popescu et al., 2019). The fetal liver HSCs mapped strongly to the WNTd CD34^{+} progenitors, whereas the yolk sac MPPs did not (Fig. S7E). In particular, the human fetal liver HSC/MPPs and the WNTd CD34^{+} progenitors expressed *HOXA9*, which is absent in the human yolk sac progenitors and the WNTi cells (Fig. S7F) (Popescu et al., 2019). *HOXA9* has previously been shown to be a crucial factor for generation of HSCs from endothelium (Zhou et al., 2016; Ng et al., 2016).

Interestingly, WNTi and WNTd cultures both contained cells expressing canonical GMP genes (*ELANE*, *MPO*, *AZU1*, *PRTN3*),

Development (2022) 149, dev200016. doi:10.1242/dev.200016

despite the WNTi culture not having a classical CD45RA$^+$ GMP population by flow cytometry (Fig. 3F, Fig. S6C). Thus, we further investigated the macrophage progenitor populations in each culture by pseudotime analysis using Palantir (Setty et al., 2019). We independently clustered the WNTd and WNTi progenitor datasets, assigned cluster identifications using the gene sets shown in Fig. S6, and superimposed pseudotime and entropy values (Fig. 4, Fig. S8A,B). We additionally plotted the probability of a cell differentiating into a macrophage or dendritic cell to identify the developmental trajectory of this lineage. Within the WNTd differentiation, CD34$^+$ progenitors displayed the lowest pseudotime and greatest entropy values, consistent with these cells being the earliest population (Fig. 4A,B). Calculation of macrophage and dendritic cell potential showed the expected developmental trajectory from GMP to monocyte to macrophage/dendritic cell (Fig. 4C). Interestingly, we found two separate WNTd monocyte populations; monocyte-1 falls between the GMP and macrophage clusters, whereas monocyte-2 falls between the CD34$^+$ progenitor and dendritic cell-like clusters (Fig. 4A, Fig. S8A). Monocyte-2 cells expressed several genes found in human dendritic cells, including *ENHO*, *CD1D*, *ITGB7*, *FGL2* and *CLEC10A*, indicating that these monocytes are likely dendritic cell progenitors. This observation is consistent with the finding in mice that monocyte-derived dendritic cells come from a monocyte-dendritic cell progenitor (MDP) that arises directly from the CMP, rather than from the GMP (Yáñez et al., 2017). The monocyte-2 gene signature is absent from the WNTi culture, consistent with the lack of a WNTi dendritic cell-like population (Fig. S8B).

The WNTi clusters with the lowest pseudotime and highest entropy values included RBC progenitors and a population of potential myeloid progenitors that clustered between megakaryocytes and monocytes (progenitor 1, Fig. 4D,E). Calculation of macrophage potential suggested that progenitor 1 has the capacity to give rise to macrophages (Fig. 4F). This analysis

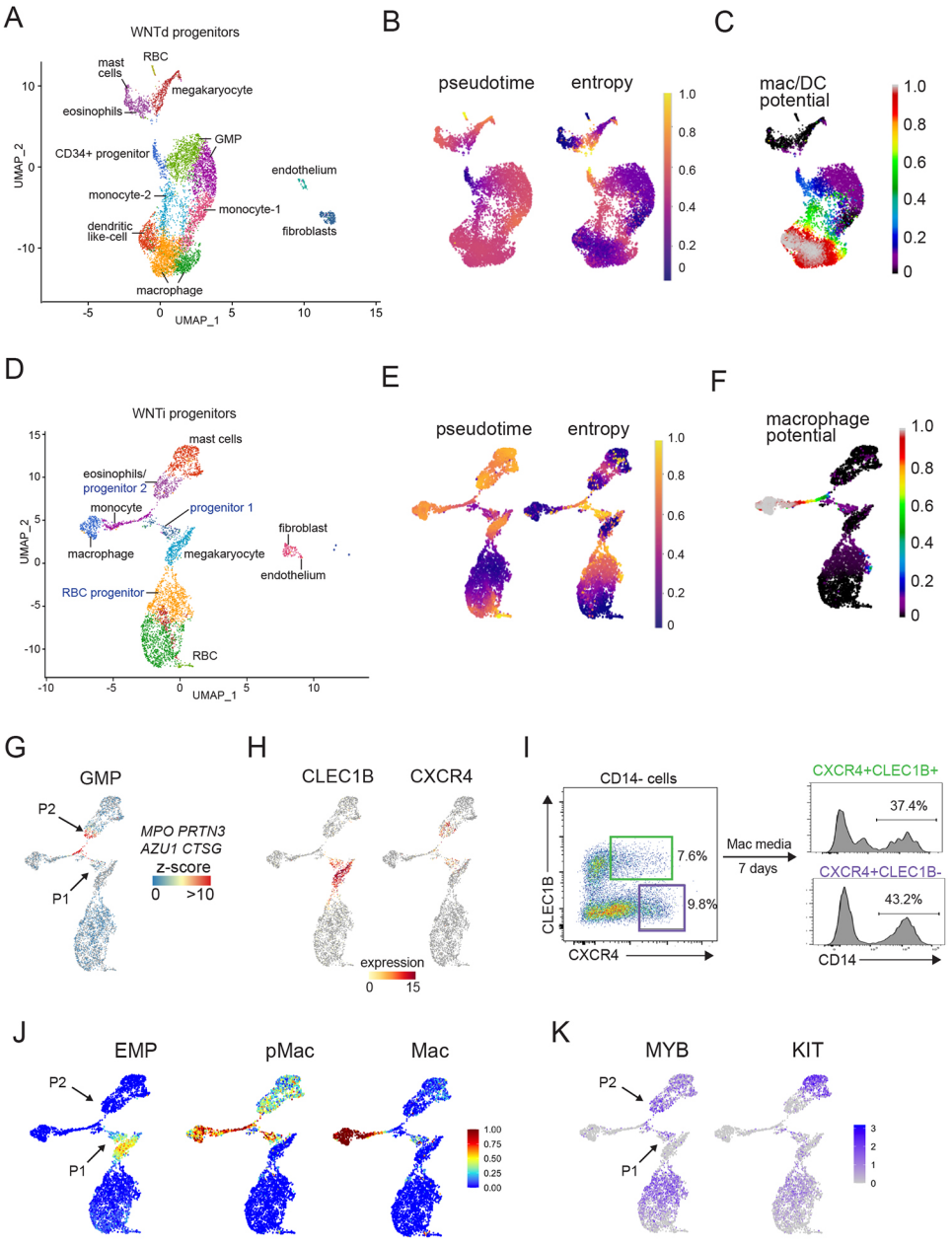

Fig. 4. Developmental paths of WNTi and WNTd macrophages. (A) scRNAseq UMAP plot of WNTd progenitor culture alone. (B) Palantir trajectory analysis of the WNTd progenitors showing pseudotime and entropy (differentiation potential). (C) Palantir imputed macrophage potential for all cells in the WNTd progenitor culture. (D) scRNAseq UMAP of WNTi progenitor culture alone. (E) Palantir trajectory analysis of the WNTi progenitors showing pseudotime and entropy. (F) Palantir imputed macrophage potential for all cells in the WNTi progenitor culture. (G) *z*-score feature plot showing expression of GMP genes in the WNTi cells. Arrows indicate progenitors 1 and 2 (P1 and P2). (H) Feature plots of *CLEC1B* and *CXCR4* expression in WNTi cells. (I) Flow cytometry plots showing CD14$^-$CXCR4$^+$CLEC1B$^-$ and CD14$^-$CXCR4$^+$CLEC1B$^+$ cells in WNTi culture after 4 days in macrophage media. Panels on the right show CD14 expression in these cultures following seven additional days in macrophage media. Results are representative of three independent experiments. (J) *z*-score plots of EMP, pMac and macrophage gene signatures from Mass et al. (2016) in the WNTi cells. Gene lists are given in Table S3. (K) Feature plots of EMP genes *MYB* and *KIT* in the WNTi progenitors.

Development (2022) 149, dev200016. doi:10.1242/dev.200016

also showed possible macrophage potential arising out of the eosinophil cluster, which contained cells expressing GMP genes (*ELANE*, *MPO*, *AZU1*, *PRTN3*) (progenitor 2, Fig. 4D,F,G). To determine whether these two progenitors can give rise to macrophages, we established a flow cytometry protocol to isolate these cell populations. Based on the scRNAseq data, we found that *CXCR4* was expressed in both progenitor 1 and 2 (Fig. 4H). As *CXCR4* is also expressed in the WNTd GMP cluster, it may be a useful marker of macrophage progenitors (Fig. S8C). The progenitor 1 cluster also expressed megakaryocyte marker *CLEC1B*. We isolated $CD14^{-}CXCR4^{+}CLEC1B^{-}$ and $CD14^{-}CXCR4^{+}CLEC1B^{+}$ cells from macrophage day 4 WNTi differentiations and cultured them in macrophage media for 7 days. The $CXCR4^{+}CLEC1B^{-}$ and $CXCR4^{+}CLEC1B^{+}$ cells both efficiently gave rise to $CD14^{+}$ cells with similar morphology, confirming their macrophage potential (Fig. 4I, Fig. S8D). Addition of stem cell factor (SCF) to macrophage media supported mast cell differentiation from both progenitor 1 and 2 (Fig. S8E). Culture in megakaryocyte-inducing conditions gave rise to $CD41^{+}CD42b^{+}$ megakaryocytes from both progenitors, with a higher percentage of $CD41^{+}CD42b^{+}$ cells in the progenitor 1 culture (Fig. S8F). When cultured under conditions supporting granulocyte differentiation, progenitor 2 gave rise to CD32 $(FCGR2)^{+}CD15^{+}CD16$ $(FCGR3)^{+}$ neutrophils, consistent with the expression of GMP genes in this cluster, whereas no $CD32^{+}$ granulocytes arose from progenitor 1 (Fig. S8G,H).

To confirm that the WNTi cells expressing GMP genes were not as result of contamination from the WNTd pathway, we isolated $KDR^{+}CD235A^{+}$ cells on day 3 of a WNTi differentiation, which have previously been shown to have exclusively extra-embryonic-like hematopoietic potential (Fig. S9A) (Sturgeon et al., 2014). We also isolated $KDR^{+}CD235A^{-}$ cells from a WNTd culture, which are exclusively intra-embryonic-like, at the same time point. These cells were differentiated as before, then $CD34^{+}CD43^{+}$ WNTi cells and $CD34^{+}CD43^{-}$ WNTd cells were isolated on day 8 and cultured in macrophage media (Fig. S9B). After 6 days of macrophage differentiation, we analyzed MPO protein expression, as a marker of the GMP gene program, and found $MPO^{+}CD14^{-}$ cells in the WNTi and the WNTd cultures (Fig. S9C). Therefore, although WNTi progenitors may not pass through a canonical GMP, based on surface expression of CD45RA, the cells arising from progenitor 2 nevertheless develop through a transitional intermediate that expresses a GMP-like gene signature. Progenitor 1, in contrast, does not contain a GMP-like population, but instead has a gene expression profile comparable to the EMP and pre-macrophages (pMac) observed in mice (Fig. 4J,K, Table S3) (Mass et al., 2016).

WNTi and WNTd macrophages are functionally distinct

We next sought to determine whether WNTi and WNTd macrophages exhibit functional differences. Tissue-resident macrophages express lower levels of inflammatory genes in response to stimuli, compared with monocyte-derived macrophages (Watanabe et al., 2019; Epelman et al., 2014a; Lavine et al., 2014). To determine whether WNTi and WNTd macrophages had intrinsically different inflammatory responses, we assayed levels of *IL1B*, *TNF* and *IL6* gene expression following treatment with lipopolysaccharide (LPS). Upon stimulation with either 2.5 ng/ml or 25 ng/ml LPS, WNTi macrophages expressed significantly lower levels of *IL1B* and *TNF* than WNTd macrophages, whereas expression of *IL6* was comparable between the two (Fig. 5A). Thus, in the context of LPS treatment, WNTi macrophages appear to be less inflammatory than WNTd macrophages.

As shown in Fig. 1, phagocytosis of *E. coli* particles was not different between WNTd and WNTi macrophages, but higher expression of *CD36* on WNTi macrophages indicated possible increased phagocytic capacity for apoptotic cells. To test this hypothesis, we incubated WNTi and WNTd macrophages with pHrodo Red-labeled apoptotic mouse thymocytes. After 2 or 5 h of co-incubation, we assayed the number of thymocytes phagocytosed by each macrophage (Fig. 5B). At both time points, a higher percentage of WNTi macrophages had phagocytosed thymocytes, compared with the WNTd macrophages. Additionally, the mean number of thymocytes phagocytosed by each WNTi macrophage was higher, yielding a higher overall phagocytic index for apoptotic cells (Fig. 5B,C).

Production of reactive oxygen species (ROS) by macrophages is a crucial component of their role in clearance of pathogens; however, it can also modulate immune responses and promote polarization of macrophages towards a reparative phenotype (Yang et al., 2019). Thus, we wanted to determine whether there are intrinsic differences in ROS production between WNTi and WNTd macrophages. We stimulated WNTi and WNTd macrophages with either serum-opsonized zymosan (SOZ) particles or phorbol 12-myristate 13-acetate (PMA) and used a luminol-based assay to detect production of ROS. WNTi macrophages produced significantly more ROS than WNTd macrophages in response to SOZ, but there was no difference in response to PMA, suggesting a specificity for increased ROS production in WNTi macrophages in response to a particulate antigen (Fig. 5D). The NBT assay showed nearly 100% positivity in both genotypes, so was not repeated on each replicate. We also did not find differences in the expression of NADPH oxidase NOX2 (*CYBB*) or potential SOZ receptors Toll-like receptor 2 (*TLR2*), Mac-1 (*ITGB2*) or dectin (*CLEC7A*) between WNTi and WNTd macrophages (Fig. S10A). Intriguingly, it has previously been shown that mouse resident peritoneal macrophages have a sustained respiratory burst in response to zymosan that is dependent on generation of ROS by the mitochondrial respiratory chain (Davies et al., 2017). The peritoneal macrophages also had increased mitochondrial respiratory capacity, compared with bone marrow derived macrophages (BMDMs), that allowed for this sustained respiratory burst. Thus, we assayed mitochondrial function in the WNTi and WNTd macrophages by measuring oxygen consumption rate (OCR) during a mitochondrial stress test. WNTi macrophages had a higher basal OCR and showed higher spare respiratory capacity (SRC) upon electron transport chain uncoupling than WNTd macrophages (Fig. 5E,F). This phenotype was amplified upon treatment with LPS. A subset of mitochondrially encoded components of the electron transport chain (*MT-ND4*, *MT-ND5*, *MT-CO2*, *MT-CYB*) are expressed at higher levels in WNTi macrophages, compared with WNTd macrophages, which may contribute to this increased respiratory capacity (Fig. S10B). Collectively, these data indicate that WNTi and WNTd macrophages have inherent differences in metabolic and inflammatory capacity that are consistent with known functional distinctions between tissue-resident and monocyte-derived macrophages.

DISCUSSION

Tissue-resident macrophages are increasingly recognized as important contributors to embryonic development, tissue maturation, remodeling and repair. To date, few systems exist to

Development (2022) 149, dev200016. doi:10.1242/dev.200016

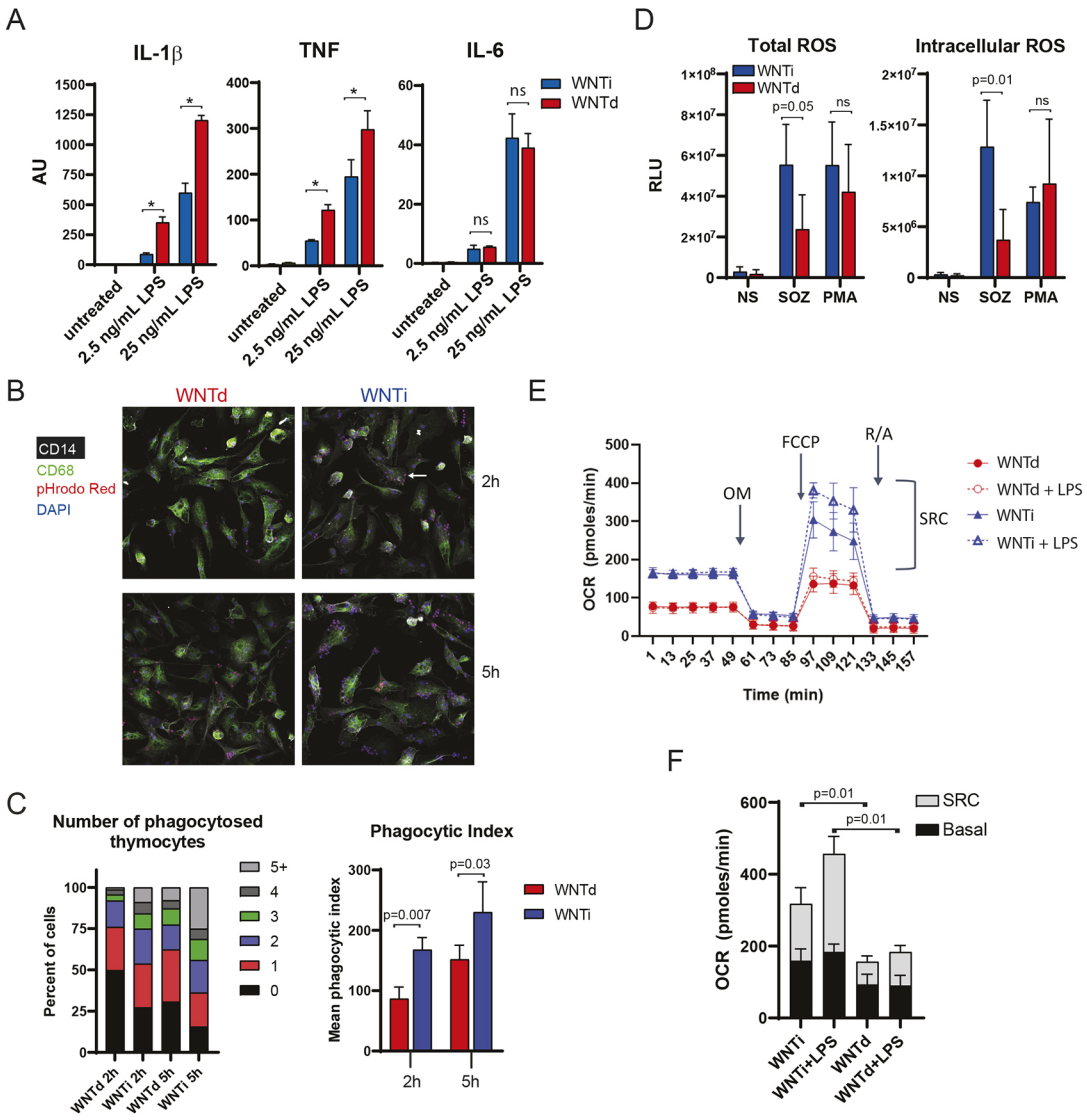

Fig. 5. Functional analysis of WNTi and WNTd macrophages. (A) Quantitative RT-PCR of *IL1B*, *TNF*, and *IL6* gene expression of in WNTi and WNTd macrophages after 4 h treatment with LPS. **P*<0.05 (two-tailed Student's *t*-test; *n*=3). (B) Representative immunofluorescence of phagocytosis of pHrodo Red-labeled apoptotic thymocytes by WNTd and WNTi macrophages. Cells are shown after co-incubation for 2 h and 5 h. Arrow indicates an example of a phagocytosed thymocyte. (C) Quantification of apoptotic thymocyte phagocytosis by WNTd and WNTi macrophages from three independent differentiations. Left graph shows the percentage of macrophages that have phagocytosed thymocytes. Right graph shows mean phagocytic index (percentage of cells with thymocytes×mean thymocytes/cell). Two-tailed Student's *t*-test. (D) Production of ROS by WNTi and WNTd macrophages during a 1 h treatment with SOZ or PMA. Left panel shows total ROS, right panel shows intracellular ROS (superoxide dismutase treated). NS, not stimulated. Two-tailed Student's *t*-test, *n*=3. ns, not significant. (E) OCR in untreated and LPS-treated (10 ng/ml) WNTi and WNTd macrophages during the Seahorse mitochondrial stress test. Representative of three experiments. FCCP, carbonyl cyanide 4-(trifluoromethoxy)phenylhydrazone; OM, oligomycin; R/A, rotenone/antimycin. (F) Quantification of mitochondrial stress tests, using the first basal OCR measurement and the first measurement following addition of FCCP for calculating SRC. Values are averages from three experiments, ±s.d. Two-tailed Student's *t*-test.

investigate tissue resident macrophage specification, function, and applicability to regenerative medicine. This technological gap is most apparent in the study of human tissue-resident macrophages, which is largely restricted to *ex vivo* and transcriptomic analyses of explanted human specimens. Recent reports have demonstrated that macrophages derived from induced pluripotent stem cells through yolk-sac-like hematopoiesis can take on microglial characteristics when co-cultured with neurons, but these have not been compared with macrophages generated through intra-embryonic-like hematopoiesis (Takata et al., 2017; Haenseler et al., 2017). By leveraging known differences in the developmental origin of tissue-resident and monocyte-derived macrophages, we established an experimentally tractable *in vitro* system to model each of these macrophage populations. We demonstrate that macrophages derived from extra-embryonic-like and intra-embryonic-like hematopoietic progenitors have unique gene expression signatures, developmental trajectories, and functions that are consistent with *in vivo* characteristics of tissue-resident and monocyte-derived macrophages, respectively.

Differences between tissue-resident macrophages and monocyte-derived macrophages have been largely ascribed to the impacts of the tissue microenvironment (Lavin et al., 2014). Although the tissue environment is certainly a major component driving behavior of tissue-resident macrophages, we show intrinsic

Development (2022) 149, dev200016. doi:10.1242/dev.200016

differences in transcriptional signatures and cellular function between extra- and intra-embryonic-like macrophage lineages. We revealed that macrophages derived from extra-embryonic-like hematopoiesis (WNTi) express a wide array of genes associated with general tissue-resident macrophage identity (Summers et al., 2020). These genes are expressed in multiple types of tissue-resident macrophages, as well as in human yolk-sac derived macrophages isolated prior to HSC formation, suggesting that the extra-embryonic macrophages that populate tissues during development are predisposed to this gene expression program (Bian et al., 2020; Popescu et al., 2019). Genes that are associated with a specific type of tissue-resident macrophage, such as Kupffer cell-associated *CLEC4A* and *CD5L* and Langerhans cell-associated *CD207*, were largely absent from both WNTi and WNTd macrophages (Summers et al., 2020).

WNTi and WNTd macrophages emerge from distinct progenitors, each with different functional capacity. The WNTd progenitors recapitulate definitive myelopoiesis, with eosinophil and megakaryocyte lineages completely separate from the monocyte and macrophage lineage, consistent with these cell types originating from distinct CMPs (Drissen et al., 2016, 2019). In contrast, the WNTi GMP-like progenitor (progenitor 2) also expressed eosinophil genes. Additionally, WNTi progenitor 1 expresses megakaryocyte genes, as has been described for yolk-sac-derived EMPs (Mass et al., 2016). This overlap between transcriptional programs in the WNTi progenitors may drive differences in gene expression and cellular function between WNTi and WNTd macrophages. The expression of *MYB* in both WNTi progenitors, the similarity of progenitor 1 to the mouse EMP, and the diversity of myeloid cell types present in the WNTi culture all support the conclusion that the WNTi culture recapitulates the EMP wave of yolk sac hematopoiesis that gives rise to the majority of fetal tissue-resident macrophages (Hoeffel et al., 2015).

Our results further demonstrate functional differences between WNTi and WNTd macrophages that may have relevance for the function of extra- and intra-embryonic-derived macrophages *in vivo*. Previous studies have shown that metabolic changes in macrophages can alter their inflammatory properties. The mitochondrial capacity we observe in WNTi macrophages recapitulates the phenotype of resident peritoneal macrophages, which are established during embryogenesis and self-renew during adulthood (Yona et al., 2013). These peritoneal macrophages have higher spare respiratory capacity than BMDMs, despite not having a greater number of mitochondria, and utilize different metabolites (Davies et al., 2017). Resident peritoneal macrophages also have higher oxygen consumption and higher ROS production in response to zymosan, and the increase in ROS was sensitive to inhibition of the mitochondrial electron transport chain (Davies et al., 2017). This study supports the possibility that metabolic differences underlie the observed increases in ROS production and spare respiratory capacity in WNTi macrophages.

In conclusion, we have established a human platform to generate distinct lineages of macrophages derived from extra-embryonic-like and intra-embryonic-like progenitors that resemble tissue-resident and monocyte-derived macrophages, respectively. This system is experimentally tractable, as it produces large numbers of cells from a renewable resource and is amenable to pharmacological and genetic manipulations. We envision that this platform will provide new opportunities to explore applications of human tissue-resident macrophages to regenerative medicine and to dissect the mechanisms that underlie tissue-resident macrophage specification, differentiation and function.

MATERIALS AND METHODS

hPSC culture and differentiation

The human embryonic stem cell (hESC) line H1 (WA01; WiCell; male) was maintained on irradiated mouse embryonic fibroblasts in hESC media, as described previously (Sturgeon et al., 2014). For differentiation, hPSCs were cultured on Matrigel-coated plasticware (BD Biosciences) for 24 h, followed by embryoid body generation. Briefly, hPSCs were dissociated with trypsin-EDTA (0.05%) treatment for 1 min, and cells were detached by scraping to form small aggregates (six to ten cells). Embryoid bodies were resuspended in SFD (Sturgeon et al., 2012) supplemented with L-glutamine (2 mM), L-ascorbic acid (1 mM), monothioglycerol (MTG, 4×10^{-4} M), holo-transferrin (150 µg/ml) and BMP4 (10 ng/ml). After 24 h, bFGF (5 ng/ml) was added to the media. At 42 h of differentiation, activin A (1 ng/ml) and either CHIR99021 (3 µM) and SB-431452 (6 µM) (to specify WNT-dependent hematopoietic progenitors) or IWP2 (3 µM) (to specify WNT-independent hematopoietic progenitors) were added to the culture. At 72 h of differentiation, embryoid bodies were washed with IMDM (Thermo Fisher) to remove WNT modulating small molecules and placed in StemPro-34 (Thermo Fisher) supplemented with L-glutamine (2 mM), ascorbic acid (1 mM), monothioglycerol (MTG; 4×10^{-4} M), holo-transferrin (150 µg/ml), VEGF (15 ng/ml) and basic fibroblast growth factor (bFGF) (5 ng/ml). On day 6 of differentiation, IL6 (10 ng/ml), IL11 (5 ng/ml) and SCF (50 ng/ml) were added to the culture. Cultures were maintained in a low-oxygen, 5% CO_2/5% O_2/90% N_2 incubator. All human recombinant factors and small molecules were purchased from R&D Systems. On day 8 of differentiation, hematopoietic progenitors were isolated by FACS on a BD FACSAria. CD34-PE/Cy7 (clone 8G12, 348791), CD43-FITC (clone 1G10, 555475), CD184-APC (clone 12G5, 555976) and CD73-PE (clone AD2, 550257) antibodies were all purchased from BD Biosciences. Human CB $CD34^+$ progenitors were isolated using CD34-APC (clone 8G12, 340441) from BD Biosciences.

Derivation of myeloid cells from hPSC hematopoietic progenitors

Isolated WNT-dependent progenitors ($CD34^+CD43^-$), WNT-independent progenitors ($CD34^+CD43^+$) and umbilical CB progenitors ($CD34^+$) were added to Matrigel-coated wells of a 24-well plate in StemPro-34 media (supplemented with L-glutamine, ascorbic acid, MTG and holo-transferrin as above) containing TPO (30 ng/ml), BMP4 (10 ng/ml), IL6 (10 ng/ml), IL11 (5 ng/ml), FLT3L (10 ng/ml), M-CSF (10 ng/ml), bFGF (5 ng/ml) and VEGF (5 ng/ml). These cells were cultured for 14 days to generate mature macrophages. For generation of additional myeloid cell types from WNTi P1 and P2, cells sorted on Mac Day 4 were cultured in media containing 50 ng/ml SCF (mast cells); 50 ng/ml G-CSF, 25 ng/ml IL3 and 1 ng/ml IL5 (granulocytes); or 50 ng/ml TPO and 25 ng/ml SCF (megakaryocytes). Granulocyte formation was also assessed by seeding 1×10^4 P1 and P2 cells in 10mL MethoCult H4034 (STEMCELL Technologies) for 9 days.

Flow cytometry of myeloid progenitors and macrophages

WNTd and WNTi myeloid progenitors were isolated by harvesting all non-adherent cells on days 5-7 of macrophage differentiation. Cells were analyzed by flow cytometry using CD123-APC (clone 6H6, 306011), CD45RA-APC/Cy7 (clone HI100, 304127), CD64-FITC (clone 10.1, 305006) and CD14-PE (clone M5E2, 301806) antibodies from BioLegend. For characterization of macrophage progenitor potential, cells were harvested on day 4 of macrophage differentiation as above, then isolated by FACS using CXCR4-APC (clone 12G5, 306509) and CLEC1B-FITC (clone AYP1, 372007) antibodies from BioLegend. Other myeloid cell types were analyzed using KIT-BV421 (clone 104D2, BioLegend 313215), CD15-APC (clone HI98/HIM1, BD Biosciences 551376), CD16-PerCP-Cy5.5 (clone 3G8, BD Biosciences 560717), CD32-PE (clone FUN-2, BioLegend 303206), CD41a-PE (clone HIP8, BD Biosciences 555467) and CD42b-APC (clone HIP1, BioLegend 303912). For analysis of MPO expression, cells were harvested on day 6 of macrophage differentiation, fixed and permeabilized using Fix&Perm Cell Permeabilization Kit from Thermo Fisher (GAS004), then stained with MPO antibody (clone MPO455-8E6, 12-1299-42) from Thermo Fisher. Mature macrophages

Development (2022) 149, dev200016. doi:10.1242/dev.200016

were characterized using CD45-PerCP/Cy5.5 (clone HI30, 304027) and CD14-APC/Cy7 (clone 63D3, 367108) from BioLegend, and MerTK-PE (clone 125518, FAB8912P) from R&D Systems. Mouse IgG1-PE isotype control for MerTK staining was 400111 from BioLegend.

scRNAseq

All non-adherent cells were harvested on day 6 or day 14 of macrophage differentiation and prepared for scRNAseq using the 3′v2 kit from 10X Genomics, following their published protocol; 10,000 cells per sample were put into the sequencing pipeline. Samples were sequenced on a HiSeq 3000 (Illumina) and read alignment was performed using the 10X Genomics Cell Ranger pipeline (Zheng et al., 2017). Downstream analyses were performed using Seurat R software package version 4.0 (http://satijalab.org/seurat/).

The following pipeline was used for the mature macrophage (day 14) dataset: The Cell Ranger counts matrix was filtered using the following QC cutoffs: (1) genes expressed in fewer than three cells were discounted; (2) cells containing fewer than 200 or greater than 5000 genes were removed as these could be potential doublets; (3) cells with a mitochondrial content of >7.5% were removed as these are potentially dying cells. Upon filtering, normalization, variance stabilization, and scaling were performed with mitochondrial percent regression using sctransform to find 3000 highly variable genes. Principal component analysis was used to find nearest neighbors and a 2D UMAP embedding was computed for all visualization purposes. DEGs were identified using the FindAllMarkers function between clusters and WNTi and WNTd macrophages. Statistically significant genes (adjusted $P<0.05$) were used to annotate clusters. DEGs between WNTi and WNTd macrophages were used to perform gene set enrichment pathway analyses using WebGestalt with the KEGG functional database (http://www.webgestalt.org/).

The following pipeline was used for the progenitor (day 6) dataset: The Cell Ranger counts matrix was filtered using the following QC cutoffs: (1) genes expressed in fewer than three cells were discounted; (2) cells containing fewer than 200 or greater than 7000 genes were removed as these could be potential doublets; (3) cells with a mitochondrial content of >7.5% were removed as these are potentially dying cells. Upon filtering, the following was carried out for WNTd+WNTi merged, WNTd, and WNTi datasets: normalization, variance stabilization, and scaling was performed with mitochondrial percent/cell cycle regression using sctransform to find 3000 highly variable genes. Principal component analysis was used to find nearest neighbors and a UMAP embedding was computed for all visualization purposes. The FindAllMarkers function in Seurat was used to perform differential gene expression testing between clusters and canonical genes were used for annotation as highlighted by violin plots, heatmaps and feature plots. Additionally, GeneSet *z*-scores were calculated for groups of genes to highlight distinct cell states. All scripts used to analyze the data herein are available on GitHub (https://github.com/jamrute/2021_MacDiff_Bredemeyer_Lavine).

Cell types present in each cluster were determined by comparing gene expression signatures with profiles in BloodSpot (Bagger et al., 2019) and the Human Protein Atlas (https://www.proteinatlas.org/).

Palantir was used to perform all pseudotime trajectory analyses in WNTd and WNTi datasets. sctransform normalized and scaled counts from the 3000 most highly variable genes were used as an input into Palantir (https://github.com/dpeerlab/Palantir). For the WNTd dataset, the $CD34^+$ progenitor cluster was used as the starting state and for the WNTi dataset, the progenitor 1 cluster was used as the starting state.

The human fetal liver and yolk sac datasets from Popescu et al. (2019) were integrated into a single data space using Harmony (Korsunsky et al., 2019). The HSC/MPP clusters from both datasets were then reference mapped onto the WNTd and WNTi progenitor datasets using a Seurat v4 pipeline.

Macrophage morphological and functional analyses

Cells were prepared and imaged by transmission electron microscopy as described by Dege et al. (2020). Antibodies recognizing CD68 (14-0688-82), TREM2 (PA5-111856) and LYVE1 (MA5-32512) were all from Thermo Fisher. Protein expression was quantitated on a per cell basis using integrated density of sum projections of 40× confocal *z*-stacks. Phagocytosis by hPSC-derived macrophages was measured using pHrodo Red *E. coli* beads (Thermo Fisher). Macrophages were cultured with pHrodo Red beads for 1 h, then analyzed for percentage of fluorescent cells by microscopy and intensity of fluorescence by flow cytometry. The assay for phagocytosis of apoptotic thymocytes was performed as described by Miksa et al. (2009), with co-incubation times of 2 h and 5 h in 4-well chamber slides (Thermo Fisher). Slides were washed with PBS three times to remove non-attached thymocytes, fixed, and stained with anti-CD68 and anti-CD14 (PA5-13305, Thermo Fisher). Expression of inflammatory genes in hPSC-derived macrophages was measured by qRT-PCR after 4 h of treatment with either 2.5 or 25 ng/ml LPS. RNA was isolated using the PureLink RNA Mini Kit (Thermo Fisher) and cDNA was generated using the High-Capacity cDNA Reverse Transcription Kit (Thermo Fisher). qRT-PCR was performed using PowerUp SYBR Green (Thermo Fisher) and human β2 microglobulin (B2M) was used as the control gene for dCt comparisons. Primer sequences are as follows: B2M-f (ACTTTGTCACAGCCCAAGATAG); B2M-r (GCAAGCAAGCAGAATTTGGAA); IL1B-f (ATGGACAAGCTGAGGAAGATG); IL1B-r (CCCATGTGTCGAAGAAGATAGG); TNFa-f (ACTTTGGAGTGATCGGCC); TNFa-r (GCTTGAGGGTTTGCTACAAC); IL6-f (AAATTCGGTACATCCTCGACGGCA); IL6-r (AGTGCCTCTTTGCTGCTTTCACAC) (f, forward; r, reverse). Analysis of ROS production was performed on 5×10^4 cells/well using lucigenin as detailed by Bagaitkar et al. (2017). Mitochondrial analysis was performed on a Seahorse XF96 (Agilent), using 7.5×10^4 cells/well, and 1.5 µM oligomycin, 0.5 µM FCCP, 0.5 µM rotenone and 0.5 µM antimycin A, as indicated in the Seahorse XF Mitochondrial Stress Test Kit protocol. LPS treatment was 10 ng/ml for 18 h. Unpaired Student's *t*-test was used for statistical analyses, and for all experiments $n=3$.

Acknowledgements

All scRNAseq samples were prepared and sequenced at the McDonnell Genome Institute at the Washington University School of Medicine. Flow cytometry and FACS sorting were carried out at the Flow Cytometry and Fluorescence Activated Cell Sorting Core Facility at the Washington University School of Medicine. Electron microscopy was performed at the Washington University Center for Cellular Imaging. The authors thank the Haniffa lab for sharing their human scRNAseq datasets.

Competing interests

The authors declare no competing or financial interests.

Author contributions

Conceptualization: A.L.B., C.M.S., K.J.L.; Methodology: A.L.B., J.M.A., A.L.K., R.A.I., L.H., C.D., J.M.L., J.D.S., J.T.H., M.C.D., C.M.S.; Formal analysis: J.M.A., A.L.K.; Investigation: A.L.B., R.A.I., L.H., S.A.L., C.D., J.M.L.; Resources: J.D.S., J.T.H., M.C.D., C.M.S.; Data curation: A.L.K.; Writing - original draft: A.L.B.; Writing - review & editing: A.L.B., J.M.A., C.M.S., K.J.L.; Visualization: A.L.B., J.M.A.; Supervision: C.M.S., K.J.L.; Project administration: C.M.S., K.J.L.; Funding acquisition: C.M.S., K.J.L.

Funding

This work was supported by the National Institutes of Health (HL138466, HL139714, HL156349, AI148877, HL145290 and HL151777), the Children's Discovery Institute (PM-LI-2019-829) and the Fondation Leducq (20CVD02). Deposited in PMC for release after 12 months.

Data availability

scRNAseq data are available at https://github.com/jamrute/2021_MacDiff_Bredemeyer_Lavine.

Peer review history

The peer review history is available online at https://journals.biologists.com/dev/article-lookup/doi/10.1242/dev.200016.

References

Ajami, B., Bennett, J. L., Krieger, C., Tetzlaff, W. and Rossi, F. M. V. (2007). Local self-renewal can sustain CNS microglia maintenance and function throughout adult life. *Nat. Neurosci.* **10**, 1538-1543. doi:10.1038/nn2014

Bäck, M., Sultan, A., Ovchinnikova, O. and Hansson, G. K. (2007). 5-Lipoxygenase-activating protein: a potential link between innate and adaptive

immunity in atherosclerosis and adipose tissue inflammation. *Circ. Res.* **100**, 946-949. doi:10.1161/01.RES.0000264498.60702.0d

Bagaitkar, J., Barbu, E. A., Perez-Zapata, L. J., Austin, A., Huang, G., Pallat, S. and Dinauer, M. C. (2017). PI(3)P-p40phox binding regulates NADPH oxidase activation in mouse macrophages and magnitude of inflammatory responses in vivo. *J. Leukoc. Biol.* **101**, 449-457. doi:10.1189/jlb.3AB0316-139R

Bagger, F. O., Kinalis, S. and Rapin, N. (2019). BloodSpot: a database of healthy and malignant haematopoiesis updated with purified and single cell mRNA sequencing profiles. *Nucleic Acids Res.* **47**, D881-DD85. doi:10.1093/nar/gky1076

Bajpai, G. and Lavine, K. J. (2019). Isolation of macrophage subsets and stromal cells from human and mouse myocardial specimens. *J. Vis. Exp.* **154**, e60015. doi:10.3791/60015

Bajpai, G., Schneider, C., Wong, N., Bredemeyer, A., Hulsmans, M., Nahrendorf, M., Epelman, S., Kreisel, D., Liu, Y., Itoh, A. et al. (2018). The human heart contains distinct macrophage subsets with divergent origins and functions. *Nat. Med.* **24**, 1234-1245. doi:10.1038/s41591-018-0059-x

Bian, Z., Gong, Y., Huang, T., Lee, C. Z. W., Bian, L., Bai, Z., Shi, H., Zeng, Y., Liu, C., He, J. et al. (2020). Deciphering human macrophage development at single-cell resolution. *Nature* **582**, 571-576. doi:10.1038/s41586-020-2316-7

Boelte, K. C., Gordy, L. E., Joyce, S., Thompson, M. A., Yang, L. and Lin, P. C. (2011). Rgs2 mediates pro-angiogenic function of myeloid derived suppressor cells in the tumor microenvironment via upregulation of MCP-1. *PLoS ONE* **6**, e18534. doi:10.1371/journal.pone.0018534

Byrum, R. S., Goulet, J. L., Griffiths, R. J. and Koller, B. H. (1997). Role of the 5-lipoxygenase-activating protein (FLAP) in murine acute inflammatory responses. *J. Exp. Med.* **185**, 1065-1075. doi:10.1084/jem.185.6.1065

Cochain, C., Vafadarnejad, E., Arampatzi, P., Pelisek, J., Winkels, H., Ley, K., Wolf, D., Saliba, A.-E. and Zernecke, A. (2018). Single-cell RNA-seq reveals the transcriptional landscape and heterogeneity of aortic macrophages in murine atherosclerosis. *Circ. Res.* **122**, 1661-1674. doi:10.1161/CIRCRESAHA.117.312509

Collison, J. (2018). MMP12 makes the cut. *Nat. Rev. Rheumatol.* **14**, 501. doi:10.1038/s41584-018-0056-y

Corjay, M. H., Kearney, M. A., Munzer, D. A., Diamond, S. M. and Stoltenborg, J. K. (1998). Antiproliferative gene BTG1 is highly expressed in apoptotic cells in macrophage-rich areas of advanced lesions in Watanabe heritable hyperlipidemic rabbit and human. *Lab. Invest.* **78**, 847-858.

Daemen, S., Gainullina, A., Kalugotla, G., He, L., Chan, M. M., Beals, J. W., Liss, K. H., Klein, S., Feldstein, A. E., Finck, B. N. et al. (2021). Dynamic shifts in the composition of resident and recruited macrophages influence tissue remodeling in NASH. *Cell Rep.* **34**, 108626. doi:10.1016/j.celrep.2020.108626

Davies, L. C., Jenkins, S. J., Allen, J. E. and Taylor, P. R. (2013). Tissue-resident macrophages. *Nat. Immunol.* **14**, 986-995. doi:10.1038/ni.2705

Davies, L. C., Rice, C. M., Palmieri, E. M., Taylor, P. R., Kuhns, D. B. and McVicar, D. W. (2017). Peritoneal tissue-resident macrophages are metabolically poised to engage microbes using tissue-niche fuels. *Nat. Commun.* **8**, 2074. doi:10.1038/s41467-017-02092-0

Deczkowska, A., Weiner, A. and Amit, I. (2020). The physiology, pathology, and potential therapeutic applications of the TREM2 signaling pathway. *Cell* **181**, 1207-1217. doi:10.1016/j.cell.2020.05.003

Dege, C., Fegan, K. H., Creamer, J. P., Berrien-Elliott, M. M., Luff, S. A., Kim, D., Wagner, J. A., Kingsley, P. D., McGrath, K. E., Fehniger, T. A. et al. (2020). Potently cytotoxic natural killer cells initially emerge from erythro-myeloid progenitors during mammalian development. *Dev. Cell* **53**, 229-39.e7. doi:10.1016/j.devcel.2020.02.016

Ditadi, A., Sturgeon, C. M., Tober, J., Awong, G., Kennedy, M., Yzaguirre, A. D., Azzola, L., Ng, E. S., Stanley, E. G., French, D. L. et al. (2015). Human definitive haemogenic endothelium and arterial vascular endothelium represent distinct lineages. *Nat. Cell Biol.* **17**, 580-591. doi:10.1038/ncb3161

Drissen, R., Buza-Vidas, N., Woll, P., Thongjuea, S., Gambardella, A., Giustacchini, A., Mancini, E., Zriwil, A., Lutteropp, M., Grover, A. et al. (2016). Distinct myeloid progenitor-differentiation pathways identified through single-cell RNA sequencing. *Nat. Immunol.* **17**, 666-676. doi:10.1038/ni.3412

Drissen, R., Thongjuea, S., Theilgaard-Mönch, K. and Nerlov, C. (2019). Identification of two distinct pathways of human myelopoiesis. *Sci. Immunol.* **4**. doi:10.1126/sciimmunol.aau7148

Ee, M. T., Kantores, C., Ivanovska, J., Wong, M. J., Jain, A. and Jankov, R. P. (2016). Leukotriene B4 mediates macrophage influx and pulmonary hypertension in bleomycin-induced chronic neonatal lung injury. *Am. J. Physiol. Lung Cell. Mol. Physiol.* **311**, L292-L302. doi:10.1152/ajplung.00120.2016

Epelman, S., Lavine, K. J., Beaudin, A. E., Sojka, D. K., Carrero, J. A., Calderon, B., Brija, T., Gautier, E. L., Ivanov, S., Satpathy, A. T. et al. (2014a). Embryonic and adult-derived resident cardiac macrophages are maintained through distinct mechanisms at steady state and during inflammation. *Immunity* **40**, 91-104. doi:10.1016/j.immuni.2013.11.019

Epelman, S., Lavine, K. J. and Randolph, G. J. (2014b). Origin and functions of tissue macrophages. *Immunity* **41**, 21-35. doi:10.1016/j.immuni.2014.06.013

Frame, J. M., McGrath, K. E. and Palis, J. (2013). Erythro-myeloid progenitors: "definitive" hematopoiesis in the conceptus prior to the emergence of hematopoietic stem cells. *Blood Cells Mol. Dis.* **51**, 220-225. doi:10.1016/j.bcmd.2013.09.006

Frank, B., Marcu, A., de Oliveira Almeida Petersen, A. L., Weber, H., Stigloher, C., Mottram, J. C., Scholz, C. J. and Schurigt, U. (2015). Autophagic digestion of Leishmania major by host macrophages is associated with differential expression of BNIP3, CTSE, and the miRNAs miR-101c, miR-129, and miR-210. *Parasit. Vectors* **8**, 404. doi:10.1186/s13071-015-0974-3

Ginhoux, F., Greter, M., Leboeuf, M., Nandi, S., See, P., Gokhan, S., Mehler, M. F., Conway, S. J., Ng, L. G., Stanley, E. R. et al. (2010). Fate mapping analysis reveals that adult microglia derive from primitive macrophages. *Science* **330**, 841-845. doi:10.1126/science.1194637

Grasso, D., Ropolo, A., Lo Ré, A., Boggio, V., Molejón, M. I., Iovanna, J. L., Gonzalez, C. D., Urrutia, R. and Vaccaro, M. I. (2011). Zymophagy, a novel selective autophagy pathway mediated by VMP1-USP9x-p62, prevents pancreatic cell death. *J. Biol. Chem.* **286**, 8308-8324. doi:10.1074/jbc.M110.197301

Haenseler, W., Sansom, S. N., Buchrieser, J., Newey, S. E., Moore, C. S., Nicholls, F. J., Chintawar, S., Schnell, C., Antel, J. P., Allen, N. D. et al. (2017). A highly efficient human pluripotent stem cell microglia model displays a neuronal-co-culture-specific expression profile and inflammatory response. *Stem Cell Rep.* **8**, 1727-1742. doi:10.1016/j.stemcr.2017.05.017

Hamidzadeh, K., Belew, A. T., El-Sayed, N. M. and Mosser, D. M. (2020). The transition of M-CSF-derived human macrophages to a growth-promoting phenotype. *Blood Adv.* **4**, 5460-5472. doi:10.1182/bloodadvances.2020002683

Haque, M., Kendal, J. K., MacIsaac, R. M. and Demetrick, D. J. (2016). WSB1: from homeostasis to hypoxia. *J. Biomed. Sci.* **23**, 61. doi:10.1186/s12929-016-0270-3

Hashimoto, D., Chow, A., Noizat, C., Teo, P., Beasley, M. B., Leboeuf, M., Becker, C. D., See, P., Price, J., Lucas, D. et al. (2013). Tissue-resident macrophages self-maintain locally throughout adult life with minimal contribution from circulating monocytes. *Immunity* **38**, 792-804. doi:10.1016/j.immuni.2013.04.004

Hoeffel, G. and Ginhoux, F. (2015). Ontogeny of tissue-resident macrophages. *Front. Immunol.* **6**, 486. doi:10.3389/fimmu.2015.00486

Hoeffel, G., Chen, J., Lavin, Y., Low, D., Almeida, F. F., See, P., Beaudin, A. E., Lum, J., Low, I., Forsberg, E. C. et al. (2015). C-Myb(+) erythro-myeloid progenitor-derived fetal monocytes give rise to adult tissue-resident macrophages. *Immunity* **42**, 665-678. doi:10.1016/j.immuni.2015.03.011

Honold, L. and Nahrendorf, M. (2018). Resident and monocyte-derived macrophages in cardiovascular disease. *Circ. Res.* **122**, 113-127. doi:10.1161/CIRCRESAHA.117.311071

Jin, S., Zhao, G., Li, Z., Nishimoto, Y., Isohama, Y., Shen, J., Ito, T., Takeya, M., Araki, K., He, P. et al. (2009). Age-related pulmonary emphysema in mice lacking alpha/beta hydrolase domain containing 2 gene. *Biochem. Biophys. Res. Commun.* **380**, 419-424. doi:10.1016/j.bbrc.2009.01.098

Kasaai, B., Caolo, V., Peacock, H. M., Lehoux, S., Gomez-Perdiguero, E., Luttun, A. and Jones, E. A. (2017). Erythro-myeloid progenitors can differentiate from endothelial cells and modulate embryonic vascular remodeling. *Sci. Rep.* **7**, 43817. doi:10.1038/srep43817

Kataoka, K., Sato, T., Yoshimi, A., Goyama, S., Tsuruta, T., Kobayashi, H., Shimabe, M., Arai, S., Nakagawa, M., Imai, Y. et al. (2011). Evi1 is essential for hematopoietic stem cell self-renewal, and its expression marks hematopoietic cells with long-term multilineage repopulating activity. *J. Exp. Med.* **208**, 2403-2416. doi:10.1084/jem.20110447

Katzenelenbogen, Y., Sheban, F., Yalin, A., Yofe, I., Svetlichnyy, D., Jaitin, D. A., Bornstein, C., Moshe, A., Keren-Shaul, H., Cohen, M. et al. (2020). 'Coupled scRNA-seq and intracellular protein activity reveal an immunosuppressive role of TREM2 in cancer. *Cell* **182**, 872-85.e19. doi:10.1016/j.cell.2020.06.032

Korsunsky, I., Millard, N., Fan, J., Slowikowski, K., Zhang, F., Wei, K., Baglaenko, Y., Brenner, M., Loh, P.-R. and Raychaudhuri, S. (2019). Fast, sensitive and accurate integration of single-cell data with Harmony. *Nat. Methods* **16**, 1289-1296. doi:10.1038/s41592-019-0619-0

Kyriakides, T. R. and Maclauchlan, S. (2009). The role of thrombospondins in wound healing, ischemia, and the foreign body reaction. *J. Cell Commun. Signal.* **3**, 215-225. doi:10.1007/s12079-009-0077-z

Lavin, Y., Winter, D., Blecher-Gonen, R., David, E., Keren-Shaul, H., Merad, M., Jung, S. and Amit, I. (2014). Tissue-resident macrophage enhancer landscapes are shaped by the local microenvironment. *Cell* **159**, 1312-1326. doi:10.1016/j.cell.2014.11.018

Lavine, K. J., Epelman, S., Uchida, K., Weber, K. J., Nichols, C. G., Schilling, J. D., Ornitz, D. M., Randolph, G. J. and Mann, D. L. (2014). Distinct macrophage lineages contribute to disparate patterns of cardiac recovery and remodeling in the neonatal and adult heart. *Proc. Natl. Acad. Sci. USA* **111**, 16029-16034. doi:10.1073/pnas.1406508111

Lux, C. T., Yoshimoto, M., McGrath, K., Conway, S. J., Palis, J. and Yoder, M. C. (2008). All primitive and definitive hematopoietic progenitor cells emerging before E10 in the mouse embryo are products of the yolk sac. *Blood* **111**, 3435-3438. doi:10.1182/blood-2007-08-107086

Malik, J., Kim, A. R., Tyre, K. A., Cherukuri, A. R. and Palis, J. (2013). Erythropoietin critically regulates the terminal maturation of murine and human

primitive erythroblasts. *Haematologica* **98**, 1778-1787. doi:10.3324/haematol.2013.087361

Manz, M. G., Miyamoto, T., Akashi, K. and Weissman, I. L. (2002). Prospective isolation of human clonogenic common myeloid progenitors. *Proc. Natl. Acad. Sci. USA* **99**, 11872-11877. doi:10.1073/pnas.172384399

Mass, E., Ballesteros, I., Farlik, M., Halbritter, F., Günther, P., Crozet, L., Jacome-Galarza, C. E., Händler, K., Klughammer, J., Kobayashi, Y. et al. (2016). Specification of tissue-resident macrophages during organogenesis. *Science* **353**. doi:10.1126/science.aaf4238

McGrath, K. E., Frame, J. M., Fegan, K. H., Bowen, J. R., Conway, S. J., Catherman, S. C., Kingsley, P. D., Koniski, A. D. and Palis, J. (2015). Distinct sources of hematopoietic progenitors emerge before HSCs and provide functional blood cells in the mammalian embryo. *Cell Rep.* **11**, 1892-1904. doi:10.1016/j.celrep.2015.05.036

Miksa, M., Komura, H., Wu, R., Shah, K. G. and Wang, P. (2009). A novel method to determine the engulfment of apoptotic cells by macrophages using pHrodo succinimidyl ester. *J. Immunol. Methods* **342**, 71-77. doi:10.1016/j.jim.2008.11.019

Minutti, C. M., Modak, R. V., Macdonald, F., Li, F., Smyth, D. J., Dorward, D. A., Blair, N., Husovsky, C., Muir, A., Giampazolias, E. et al. (2019). A macrophage-pericyte axis directs tissue restoration via Amphiregulin-induced transforming growth factor beta activation. *Immunity* **50**, 645-54.e6. doi:10.1016/j.immuni.2019.01.008

Murray, P. J. and Wynn, T. A. (2011). Protective and pathogenic functions of macrophage subsets. *Nat. Rev. Immunol.* **11**, 723-737. doi:10.1038/nri3073

Ng, E. S., Azzola, L., Bruveris, F. F., Calvanese, V., Phipson, B., Vlahos, K., Hirst, C., Jokubaitis, V. J., Yu, Q. C., Maksimovic, J. et al. (2016). Differentiation of human embryonic stem cells to HOXA(+) hemogenic vasculature that resembles the aorta-gonad-mesonephros. *Nat. Biotechnol.* **34**, 1168-1179. doi:10.1038/nbt.3702

Palis, J. and Yoder, M. C. (2001). Yolk-sac hematopoiesis: the first blood cells of mouse and man. *Exp. Hematol.* **29**, 927-936. doi:10.1016/S0301-472X(01)00669-5

Palis, J., McGrath, K. E. and Kingsley, P. D. (1995). Initiation of hematopoiesis and vasculogenesis in murine yolk sac explants. *Blood* **86**, 156-163. doi:10.1182/blood.V86.1.156.bloodjournal861156

Palis, J., Robertson, S., Kennedy, M., Wall, C. and Keller, G. (1999). Development of erythroid and myeloid progenitors in the yolk sac and embryo proper of the mouse. *Development* **126**, 5073. doi:10.1242/dev.126.22.5073

Pina, C., May, G., Soneji, S., Hong, D. and Enver, T. (2008). MLLT3 regulates early human erythroid and megakaryocytic cell fate. *Cell Stem Cell* **2**, 264-273. doi:10.1016/j.stem.2008.01.013

Popescu, D.-M., Botting, R. A., Stephenson, E., Green, K., Webb, S., Jardine, L., Calderbank, E. F., Polanski, K., Goh, I., Efremova, M. et al. (2019). Decoding human fetal liver haematopoiesis. *Nature* **574**, 365-371. doi:10.1038/s41586-019-1652-y

Puranik, A. S., Leaf, I. A., Jensen, M. A., Hedayat, A. F., Saad, A., Kim, K.-W., Saadalla, A. M., Woollard, J. R., Kashyap, S., Textor, S. C. et al. (2018). Kidney-resident macrophages promote a proangiogenic environment in the normal and chronically ischemic mouse kidney. *Sci. Rep.* **8**, 13948. doi:10.1038/s41598-018-31887-4

Setty, M., Kiseliovas, V., Levine, J., Gayoso, A., Mazutis, L. and Pe'er, D. (2019). Characterization of cell fate probabilities in single-cell data with Palantir. *Nat. Biotechnol.* **37**, 451-460. doi:10.1038/s41587-019-0068-4

Sturgeon, C. M., Chicha, L., Ditadi, A., Zhou, Q., McGrath, K. E., Palis, J., Hammond, S. M., Wang, S., Olson, E. N. and Keller, G. (2012). Primitive erythropoiesis is regulated by miR-126 via nonhematopoietic Vcam-1+ cells. *Dev. Cell* **23**, 45-57. doi:10.1016/j.devcel.2012.05.021

Sturgeon, C. M., Ditadi, A., Awong, G., Kennedy, M. and Keller, G. (2014). Wnt signaling controls the specification of definitive and primitive hematopoiesis from human pluripotent stem cells. *Nat. Biotechnol.* **32**, 554-561. doi:10.1038/nbt.2915

Subramanian Vignesh, K. and Deepe, G. S.Jr. (2017). Metallothioneins: emerging modulators in immunity and infection. *Int. J. Mol. Sci.*, **18**, 2197. doi:10.3390/ijms18102197

Summers, K. M., Bush, S. J. and Hume, D. A. (2020). Network analysis of transcriptomic diversity amongst resident tissue macrophages and dendritic cells in the mouse mononuclear phagocyte system. *PLoS Biol.* **18**, e3000859. doi:10.1371/journal.pbio.3000859

Takata, K., Kozaki, T., Lee, C. Z. W., Thion, M. S., Otsuka, M., Lim, S., Utami, K. H., Fidan, K., Park, D. S., Malleret, B. et al. (2017). Induced-pluripotent-stem-cell-derived primitive macrophages provide a platform for modeling tissue-resident macrophage differentiation and function. *Immunity* **47**, 183-98.e6. doi:10.1016/j.immuni.2017.06.017

Watanabe, S., Alexander, M., Misharin, A. V. and Budinger, G. R. S. (2019). The role of macrophages in the resolution of inflammation. *J. Clin. Invest.* **129**, 2619-2628. doi:10.1172/JCI124615

Wynn, T. A., Chawla, A. and Pollard, J. W. (2013). Macrophage biology in development, homeostasis and disease. *Nature* **496**, 445-455. doi:10.1038/nature12034

Yáñez, A., Coetzee, S. G., Olsson, A., Muench, D. E., Berman, B. P., Hazelett, D. J., Salomonis, N., Grimes, H. L. and Goodridge, H. S. (2017). Granulocyte-monocyte progenitors and monocyte-dendritic cell progenitors independently produce functionally distinct monocytes. *Immunity* **47**, 890-902.e4. doi:10.1016/j.immuni.2017.10.021

Yang, W., Tao, Y., Wu, Y., Zhao, X., Ye, W., Zhao, D., Fu, L., Tian, C., Yang, J., He, F. et al. (2019). Neutrophils promote the development of reparative macrophages mediated by ROS to orchestrate liver repair. *Nat. Commun.* **10**, 1076. doi:10.1038/s41467-019-09046-8

Yokomizo, T., Watanabe, N., Umemoto, T., Matsuo, J., Harai, R., Kihara, Y., Nakamura, E., Tada, N., Sato, T., Takaku, T. et al. (2019). Hlf marks the developmental pathway for hematopoietic stem cells but not for erythro-myeloid progenitors. *J. Exp. Med.* **216**, 1599-1614. doi:10.1084/jem.20181399

Yona, S., Kim, K.-W., Wolf, Y., Mildner, A., Varol, D., Breker, M., Strauss-Ayali, D., Viukov, S., Guilliams, M., Misharin, A. et al. (2013). Fate mapping reveals origins and dynamics of monocytes and tissue macrophages under homeostasis. *Immunity* **38**, 79-91. doi:10.1016/j.immuni.2012.12.001

Zaiss, D. M. W., Gause, W. C., Osborne, L. C. and Artis, D. (2015). Emerging functions of amphiregulin in orchestrating immunity, inflammation, and tissue repair. *Immunity* **42**, 216-226. doi:10.1016/j.immuni.2015.01.020

Zeng, Y., He, J., Bai, Z., Li, Z., Gong, Y., Liu, C., Ni, Y., Du, J., Ma, C., Bian, L. et al. (2019). Tracing the first hematopoietic stem cell generation in human embryo by single-cell RNA sequencing. *Cell Res.* **29**, 881-894. doi:10.1038/s41422-019-0228-6

Zhang, J. and Ney, P. A. (2009). Role of BNIP3 and NIX in cell death, autophagy, and mitophagy. *Cell Death Differ.* **16**, 939-946. doi:10.1038/cdd.2009.16

Zheng, G. X. Y., Terry, J. M., Belgrader, P., Ryvkin, P., Bent, Z. W., Wilson, R., Ziraldo, S. B., Wheeler, T. D., McDermott, G. P. and Zhu, J. (2017). Massively parallel digital transcriptional profiling of single cells. *Nat. Commun.* **8**, 14049. doi:10.1038/ncomms14049

Zhong, S., Li, L., Zhang, Y.-L., Zhang, L., Lu, J., Guo, S., Liang, N., Ge, J., Zhu, M., Tao, Y. et al. (2019). Acetaldehyde dehydrogenase 2 interactions with LDLR and AMPK regulate foam cell formation. *J. Clin. Invest.* **129**, 252-267. doi:10.1172/JCI122064

Zhou, F., Li, X., Wang, W., Zhu, P., Zhou, J., He, W., Ding, M., Xiong, F., Zheng, X., Li, Z. et al. (2016). Tracing haematopoietic stem cell formation at single-cell resolution. *Nature* **533**, 487-492. doi:10.1038/nature17997